

Introducing VO²⁺ Group in Phosphomolybdic Acid and Supporting on MOF-808 for Efficient Oxidative Desulfurization

Yi Ping, Meng-Ya Zong, Zhe Zhao, Chuan-Jiao Wang, and Dan-Hong Wang*

Cite This: *ACS Omega* 2023, 8, 37421–37430

Read Online

ACCESS |



Metrics & More

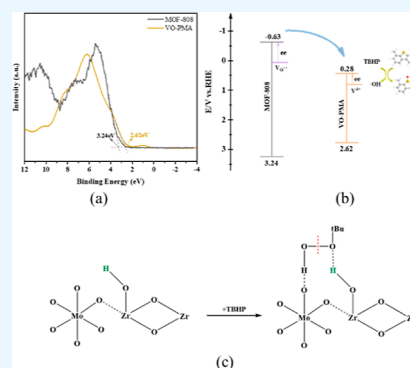


Article Recommendations



Supporting Information

ABSTRACT: Herein, by introducing a VO²⁺ group into the microstructure of phosphomolybdic acid (PMA) and loading it onto MOF-808, a series of composite catalysts were obtained by reducing the V element with Vitamin C (ascorbic acid). V atoms exist in the secondary structural units of phosphomolybdic acid as [VO(H₂O)₅]-H[PMo₁₂O₄₀]. Surprisingly, the VC-VO-PMA/MOF-808 completely removed DBT and 4,6-DMDBT from the simulated oil in 12 min. The EPR and XPS results verify the electronic structure and valence state of V⁴⁺ in the composites. The oxygen vacancy and V⁴⁺ generated by VC modification in VC-VO-PMA/MOF-808 have positive effects on the oxidation desulfurization (ODS) activity. Based on the design of the microstructure and electronic structure, this study provides a new paradigm for the development of readily available and efficient ODS catalysts.



1. INTRODUCTION

The sulfides in gasoline and diesel mainly include aliphatic sulfur compounds¹ and aromatic sulfur compounds.² SO_x produced by the combustion of sulfur compounds in gasoline and diesel not only pollutes the atmosphere but also causes irreversible harm to humans, animals, and plants.³ A certain strategy has been used to remove sulfur compounds in gasoline and diesel. Industrial hydrodesulfurization (HDS) technology provides simple removal of aliphatic sulfides (e.g., mercaptans, sulfides, etc.).⁴ However, HDS is not currently an ideal reaction path for the effective removal of all sulfides, especially aromatic sulfur compounds.^{5,6} Moreover, it must be mentioned that HDS is carried out at high temperature and high hydrogen pressure with high energy consumption, and the fatal disadvantage of HDS is the reduction in the octane number of gas oil.⁷ In contrast, oxidative desulfurization (ODS^{8–11}) carries out under a relatively mild condition, not only reduces the energy consumption of the desulfurization process but also improves the desulfurization efficiency.¹² ODS has received more and more attention in recent years.^{13,14}

The composites of polyoxometalates (POMs¹⁵) and metal–organic frameworks (MOFs¹⁶) are considered as promising catalysts for the ODS reaction.¹⁷ These POMs include heteropolyanions XM₁₂O₄₀^{m–}, in which the most common metal atoms are M = Mo⁶⁺ or W⁶⁺, and X = P⁵⁺ or Si⁴⁺ are the typically central atom.^{18,19} Keggin-type POMs have been reported to have catalytic effects in many fields due to their good structure stability and chemical tunability.^{20,21} HPMo_x@MOF-199,²² PMo₁₂@UiO-67,²³ and [Bmim]₃PMo₁₂O₄₀/UiO-66²⁴ have been proved to be effective catalysts for ODS.¹⁰ Chu et al. first coordinated formic acid on Ce to prepare MOF-

808 (Ce) and then treated it with acid to obtain MOF-808-F-H with unsaturated metal sites, which showed good performance in the ODS reaction, and the TOF value of DBT removal reached 180.3 h⁻¹ at 50 °C because MOF-808-F-H can interact with oxidants to produce active substances that promote DBT oxidation.²⁵ Mao et al. synthesized a porous phosphomolybdate-based poly IL catalyst (PDIM-PMo-W70%) based on PMA and poly[3-dodecyl-1-vinylimidazole] bromide (PDIMBr) by ion self-assembly, the DBT conversion rate could reach 100%, the closed water in the micropores may undergo structural recombination, resulting in changes in entropy enthalpy compensation, and the water cluster helped the transport of H₂O₂, which greatly promoted the formation of catalytic activity of polyacid peroxide and thus improved ODS reactivity.²⁶ Wang et al. synthesized vanadium-substituted POMs.²⁷ Zhu et al. successfully prepared a group of imidazole-polyether sulfone ionic liquids with different numbers of vanadium atoms and different kinds of imidazole cations by the facile ion exchange method.²⁸ However, in these methods, Mo atoms are replaced by V atoms or other groups, which is not conducive to the retention of Mo atoms as important catalytic active sites. Furthermore, the synergistic effect by introducing a V atom into the structure of Mo-POM is not very well understood.

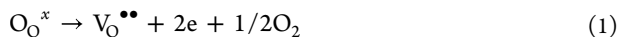
Received: July 26, 2023

Accepted: September 18, 2023

Published: September 28, 2023

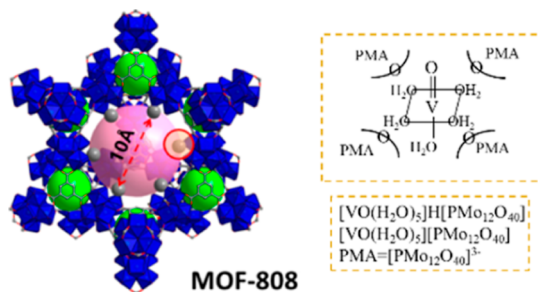


To the best of our knowledge, it is of great importance for the ODS reaction to introduce an oxygen vacancy in the MOF structure of the POMs/MOFs composites.²⁹ We have reported that Zr-MOF easily loses lattice oxygen atoms to form oxygen vacancies with electrons trapped in as eq 1.²⁴



Deng et al. found that oxygen vacancies in 26-faceted polyhedral high entropy oxide MnNiCuZnCoO_x-1000 could significantly promote the ODS effect.³⁰ Zou et al. immobilized molybdenum dioxide containing oxygen vacancies on electron-rich nitrogen-doped carbon nanotubes, and obtained great activity and renewability in ODS.³¹ By adjusting spatial confining effect and electronic confining effect of V-MOF, Chang et al. designed the confinement of MoO₄²⁻ into V-MOF³² reasonably to obtain the composite material with oxygen vacancy and V⁴⁺, which exhibits great performance in the ODS reaction.³² However, most of these composite methods are expensive and complicated, and are difficult to apply in actual industrial production. Therefore, we designed a simple and accessible strategy to produce oxygen vacancy and V⁴⁺ in POMs/MOFs composites. Herein, we innovatively loaded PMA and VO-PMA on MOF-808 (Scheme 1)³⁴ and

Scheme 1. Structures of MOF-808 and VO-PMA for Forming the VC-VO-PMA/MOF-808 Composite^a



^aGreen and pink spheres represent the tetrahedral- and adamantane-shaped cages in the framework, respectively. The dark gray balls in the framework represent the coordinated anions. For MOF-808, the diameter of the hexagonal windows is about 10 Å.³³

then modified them with Vitamin C (VC) to obtain a series of composite catalysts. MOF-808 shows a pore diameter of 10 Å, which is just enough to spatially confine one PMA molecule with a size of 10 Å, to study the synergistic effect between PMA derivatives and MOF-808 thus became very interesting. The POMs/MOFs composite catalysts were applied to the ODS reaction. It is found that VC-VO-PMA/MOF-808 efficiently removed DBT^{35,36} and 4,6-DMDBT in simulated oil compared with other catalysts. Characterization results, such as EPR and UV demonstrate that VC-VO-PMA/MOF-808 contains oxygen vacancies and V⁴⁺. The results prove that V⁴⁺ and the oxygen vacancies generated by VC modification have a positive effect on the ODS activity. This study provides a new idea for the development of facile and efficient catalysts for ODS.

2. RESULTS AND DISCUSSION

2.1. Characterization Results. It can be seen very clearly in the TEM images in Figure S1 that both MOF-808 and the composite catalysts exhibit regular octahedral morphology. The size of the nanoparticles is about 50–100 nm. SEM

images in Figure S2 can also clearly show that the catalyst has a regular morphology and a uniform size. As is shown in Figure 1, C, Mo, O, Zr, and V elements are well dispersed in the composites. The results indicate that PMA and VO-PMA are uniformly confined into MOF-808 to form the composite catalysts. The nitrogen adsorption–desorption isotherms and pore size distribution curves of the catalysts are listed in Figure S4. The samples all showed typical type I isotherms, indicating a microporous structure. Accordingly, the pore size distribution computed by the Horvath–Kawazoe method is distributed in 5 and 8–10 Å, in which the calculated 10 Å pore is very consistent. The BET surface area and pore volume of the samples are summarized in Table S1. The BET surface area of VC-VO-PMA/MOF-808 samples is similar to that of the MOF-808 samples and higher than that of the VO-PMA/MOF-808 samples. The TGA curves shown in Figure S5 demonstrate that the skeleton of the samples collapses at 500–600 °C.

The samples were subjected to powder X-ray diffraction (PXRD) analysis, and the results are presented in Figures 2a and S3. Diffraction peaks were detected at 4.3, 8.4, and 8.7° for all samples. This is consistent with MOF-808, indicating that a series of composite catalysts with MOF-808 structure as the support were successfully synthesized. After the introduction of PMA and VO-PMA into the micropore of MOF-808, the framework of MOF-808 did not destroy. Furthermore, the MOF-808 structure in the composite catalysts is also maintained after modification PMA and VO-PMA with VC. Inductively coupled plasma-optical emission spectroscopy (ICP-OES) was performed to accurately obtain the contents of each element in the composites in Table 1. The presence of P, Mo, and V elements implied that PMA and VO-PMA were successfully loaded on MOF-808. As expected, the content of Mo element in PMA/MOF-808 and VO-PMA/MOF-808 is roughly the same, that the amount of effective active site is similar. Moreover, the content of Mo element in PMA/MOF-808 and VC-PMA/MOF-808 is similar, which proves that the process of VC modification will not cause the loss of Mo species. The similar Mo and V contents of VO-PMA/MOF-808 and VC-VO-PMA/MOF-808 also support this conclusion.

The infrared (IR) spectra results of PMA and VO-PMA are listed in Figure 2b. The results show that VO-PMA maintains a similar Keggin structure to PMA. The peaks at 1065, 963, 869, and 785 cm⁻¹ can be respectively explained by the stretching vibrations of P–O_a, Mo = O_b, Mo–O_b–Mo, and Mo–O_c–Mo (O_a, O_b, O_c, and O_d represent oxygen atoms at different positions in PMA).³⁷ VO-PMA also shows the same vibration characteristics in these positions, which gives evidence to the Keggin structure of VO-PMA. The band at 1665 cm⁻¹ in MOF-808 can be assigned to the carbonyl group (C = O) in DMF. It is obvious that this peak disappears in the composites, which indicates that PMA/VO-PMA may substitute the position of the neutral molecular such as DMF adsorbed on MOF-808. The bands at 885 cm⁻¹ can be attributed to Mo–O–Mo (bridging oxygen) in PMA or VO-PMA.

The slight shift of the bands from 869 to 885 cm⁻¹ can provide preliminary evidence of the interaction between PMA/VO-PMA and MOF. The bands at 1577 and 1381 cm⁻¹ are attributed to the asymmetric and symmetric stretching vibration of carboxyl groups of BTC, respectively.³⁸ The shifts of these two bands in VC-PMA/MOF-808 and VC-VO-PMA/MOF-808 also provide evidence of the interaction between PMA/VO-PMA and MOF-808. The results of XPS are

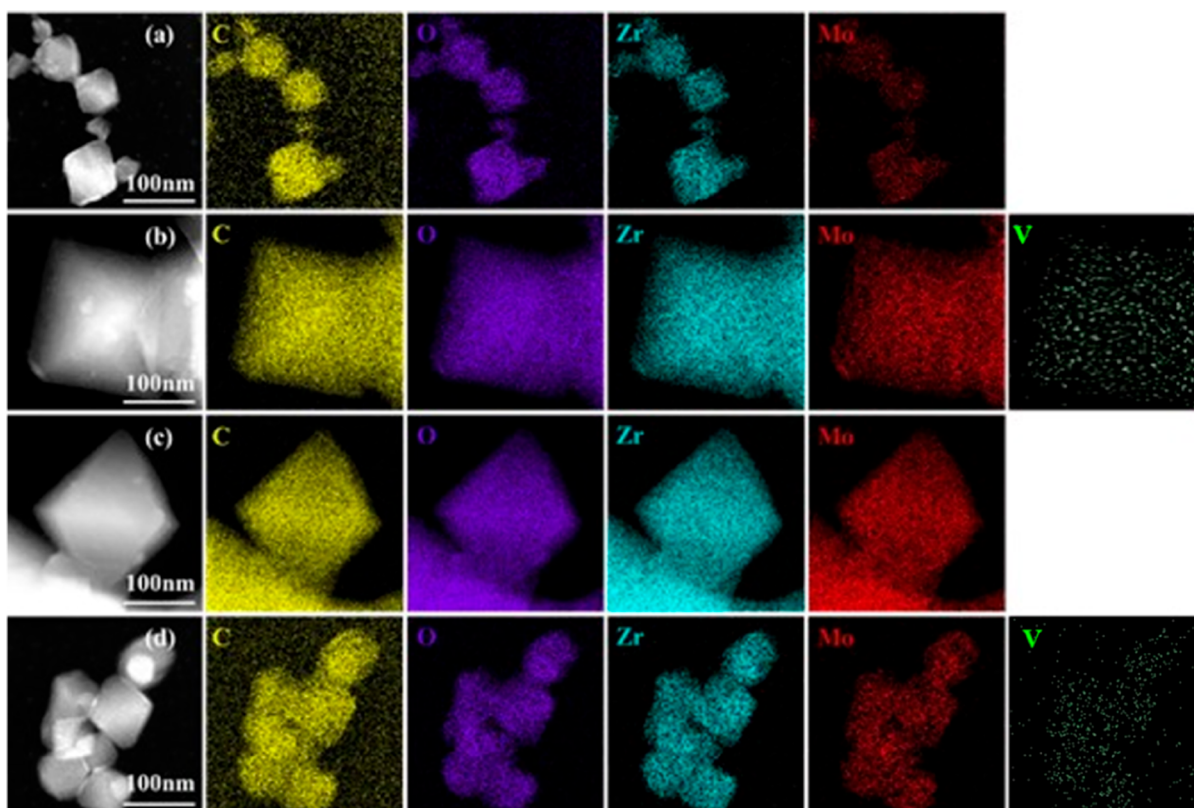


Figure 1. TEM element mapping of different samples. (a) PMA/MOF-808, (b) VO-PMA/MOF-808, (c) VC-PMA/MOF-808, and (d) VC-VO-PMA/MOF-808.

presented in Figures 2c-f and S6. All data are corrected by the binding energy (BE) of C 1s at 284.8 eV. Compared with PMA/MOF-808 and VO-PMA/MOF-808, the O 1s of VC-PMA/MOF-808 and VC-VO-PMA/MOF-808 show stronger peaks at higher BE of about 531.5 eV. This indicates that the modification by VC may lead to the generation of oxygen vacancy defects. Considering that VC is a gentle reducing agent, whether Mo^{5+} will be produced in the composite must be verified. It is clear in the Figure 2d that there is no obvious peak at the 230.4 eV.³⁷ Therefore, we boldly hypothesized that the reduction by VC resulted in the generation of oxygen vacancies in the composites (oxygen vacancies can also be detected by EPR subsequently) and V^{4+} (V^{4+} cannot be detected by XPS in the composites due to the low content and can be verified by EPR subsequently) without reducing the Mo^{6+} to Mo^{5+} . The slight difference between P 2p of PMA and P 2p of VO-PMA proves that the presence of a V atom has an effect on the P atom in the Keggin structure, which may lead to different activities of the composites in the ODS catalytic reactions. Furthermore, compared with PMA and VO-PMA, the P 2p peaks and Mo 3d peaks in the composites shifted in the lower BE direction. The result proves the interaction of PMA and VO-PMA with MOF-808, that is, the electron density around P and Mo atoms in PMA/VO-PMA increased by the formation of the Mo–O–Zr bond with MOF-808. The fine spectrum of Zr 3d did not change significantly in the catalysts, proving the stability of the support material MOF-808 in composite catalysts. The fitting spectra of V 2p in pure VO-PMA are given in Figure S6. Both V^{5+} and V^{4+} exists in VO-PMA. Thus, both $[\text{VO}]\text{PMo}_{12}\text{O}_{40}$ and $[\text{VO}]\text{HPMo}_{12}\text{O}_{40}$ are possible chemical formula for VO-PMA.³⁹ Due to the low content of element V in the composites, its spectrum was

unfortunately not obtained in XPS. The changes of the chemical valence of V elements can be proved by EPR below.

To illustrate the existence of oxygen vacancies, the composite catalysts were characterized by electron paramagnetic resonance spectroscopy (EPR). The results are shown in Figure 3a, and it can be seen that there is a small signal for MOF-808 and PMA/MOF-808 at $g = 2.004$. The EPR signal of VC-PMA/MOF-808 after VC modification is obviously stronger. Therefore, it can be inferred that the addition of VC increases the number of vacancy defects in the composites. The V^{4+} will show a split EPR signal around $g = 2.004$, which affects the judgment of the existence of oxygen vacancy in VO-PMA and its composite. Thus, the EPR results of VO-PMA and its composites are given in Figure 3b. It is shown that V^{4+} with split EPR peaks exists in the composites. V^{4+} exhibits hyperfine structure resulting from the interaction of the nuclear magnetic moment with the free electron ($3d^1$).⁴⁰ Furthermore, VC-VO-PMA/MOF-808 modified by VC has obviously stronger V^{4+} signals than VO-PMA/MOF-808. The results demonstrate that V^{5+} is reduced to V^{4+} by VC in the composites. We have reported³⁰ that V^{4+} promote ODS activity compared with V^{5+} . EPR results provide strong evidence of the existence of oxygen vacancy and V^{4+} , which act as the active sites for the ODS reaction. ^{31}P , ^{13}C , and ^1H NMR were collected and are given in Figure 3d,e,f. For PMA and VO-PMA, a strong ^{31}P peak can be observed at a chemical shift of -8 ppm, which is close to the Keggin structural feature of $[\text{PMo}_{12}\text{O}_{40}]^{3-}$. The broadened ^{31}P signals of the composites transfer to the high field at ~ -10 ppm, which is due to the electron density around P elements increases significantly. This result is consistent with the XPS result that electron transfer from MOF-808 to PMA/VO-PMA leads to lower BEs of Mo

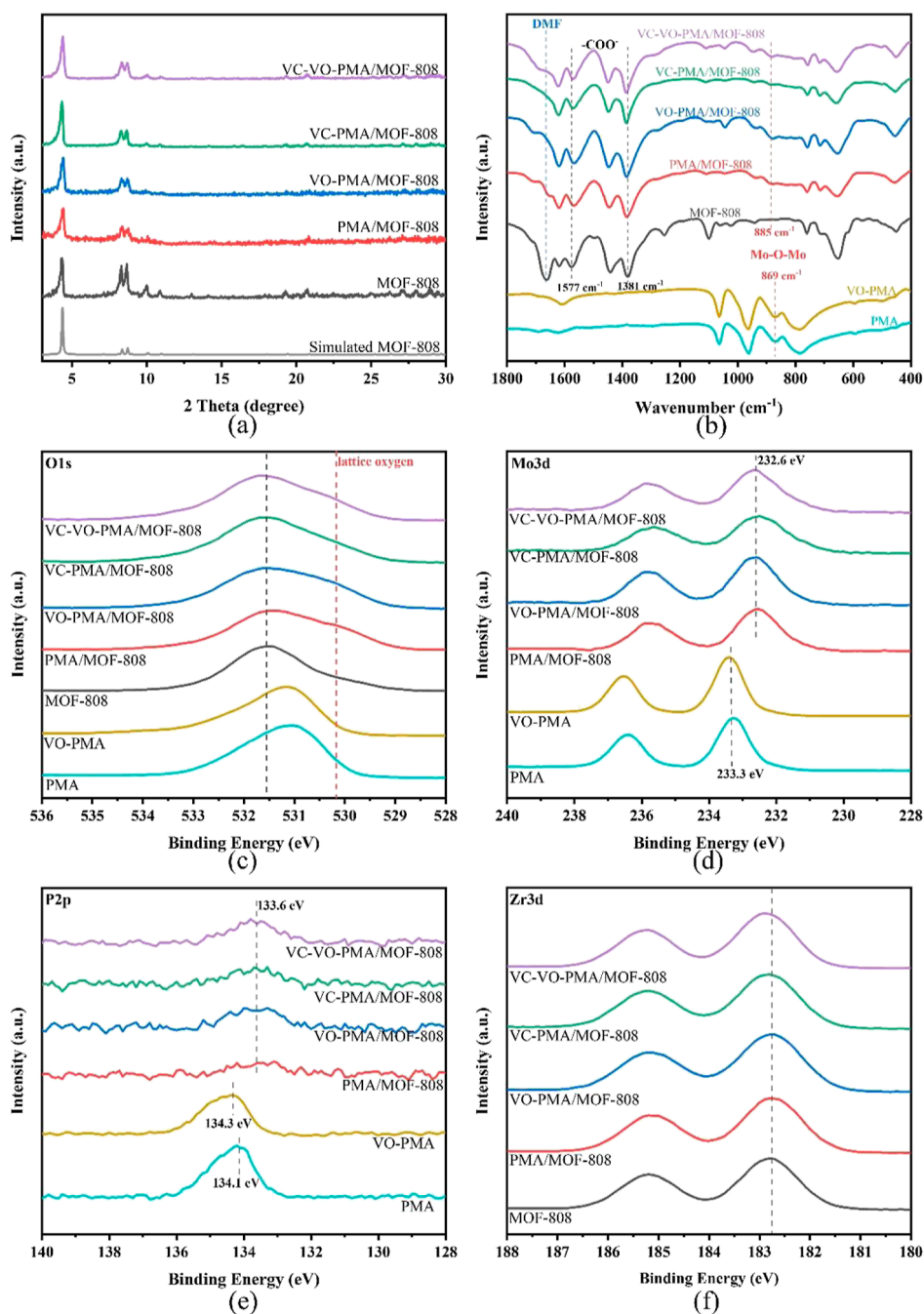


Figure 2. (a) PXRD, (b) IR, and (c–f) XPS results of the samples.

Table 1. ICP-OES Results of the Samples

sample	Zr (wt %)	Mo (wt %)	V (wt %)
PMA/MOF-808	30.8	7.52	
VO-PMA/MOF-808	28.8	8.44	0.286
VC-PMA/MOF-808	30.5	7.51	
VC-VO-PMA/MOF-808	31.9	7.18	0.158

3d in the composites. The two main signals in ^{13}C NMR at 170 and 134 ppm are derived from carboxyl C in COO^- and benzene C, respectively.⁴¹ The broaden signal at 8.7 ppm in Figure 3d can be attributed to H atoms in the aromatic ring of BTC linkers.⁴² After PMA/VO-PMA loading, the chemical environment for C and H atoms in the BTC linkers slightly changes.

The acid–base titration curve and first derivative curve for different samples are shown in Figure S7. The structural formula of perfect MOF-808 can be represented by $\text{Zr}_6\text{O}_4(\text{OH})_4(\text{BTC})_2(\text{CH}_3\text{COO})_6$.⁴³ All the samples have two distinct titration jump points which can be seen from the first derivative of the titration curves ($\text{pK}_a = 3.3$ and 6.8 respectively, as shown in Table S2). By analyzing the structure of the catalysts, it can be assumed that $\mu\text{-OH}$ ($\text{pK}_a = 3.3$) and the unsaturated Zr sites with the terminal Zr-OH ($\text{pK}_a = 6.8$) are responsible for the two titration jump points, respectively.^{44,45} Zr-OH is related to the unsaturated metal sites resulting from the competitive coordination of acetic acid and BTC during the synthesis. This result illustrates the presence of an unsaturated Zr site in the catalysts, which is consistent

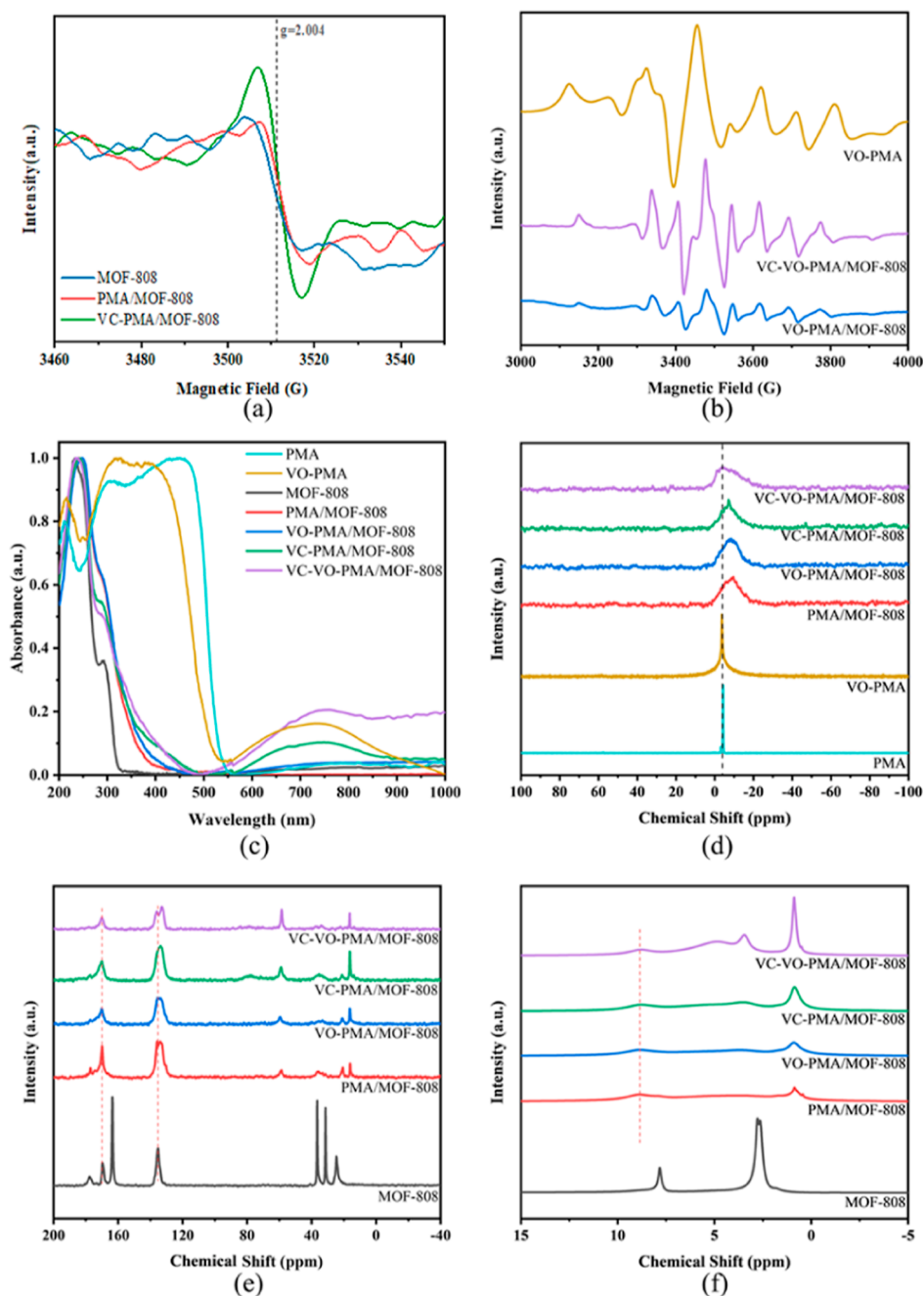


Figure 3. (a,b) EPR spectra, (c) UV–vis DRS spectra, and (d) ^{31}P , (e) ^{13}C , and (f) ^1H NMR spectra of the samples.

with the conclusion of EPR spectra. UV–vis diffuse reflectance spectrum (UV–vis DRS) is also often able to demonstrate oxygen vacancies in the composites. As shown in the Figure 3c, VO-PMA, VC-PMA/MOF-808, and VC-VO-PMA/MOF-808 exhibit obvious absorption at 600–800 nm compared to PMA, indicating the presence of V^{4+} and trapped electrons in the oxygen vacancies as eq 1 described.

Since the oxygen vacancies captured by electrons can result in electron transition, adsorption bands can be observed in the 600–800 nm region. This result together with the EPR results proves that VC modification causes oxygen vacancies in the composites. It is also worth noting that the absorption of VC-VO-PMA/MOF-808 at 600–800 nm is stronger than that of VC-PMA/MOF-808, which can be assigned to the V 3d electron transition also occurred with d^1 electron in V^{4+} .

Moreover, according to the relationship between the absorption edge (λ) and the energy bandwidth of each sample ($E_g = 1240/\lambda$), the energy band widths were calculated and listed in Table 2. After VC modification, the band gap

Table 2. Band Gap of the Samples

sample	band gap (eV)
PMA	2.33
VO-PMA	2.34
MOF-808	3.87
PMA/MOF-808	3.27
VO-PMA/MOF-808	3.16
VC-PMA/MOF-808	2.55
VC-VO-PMA/MOF-808	2.61

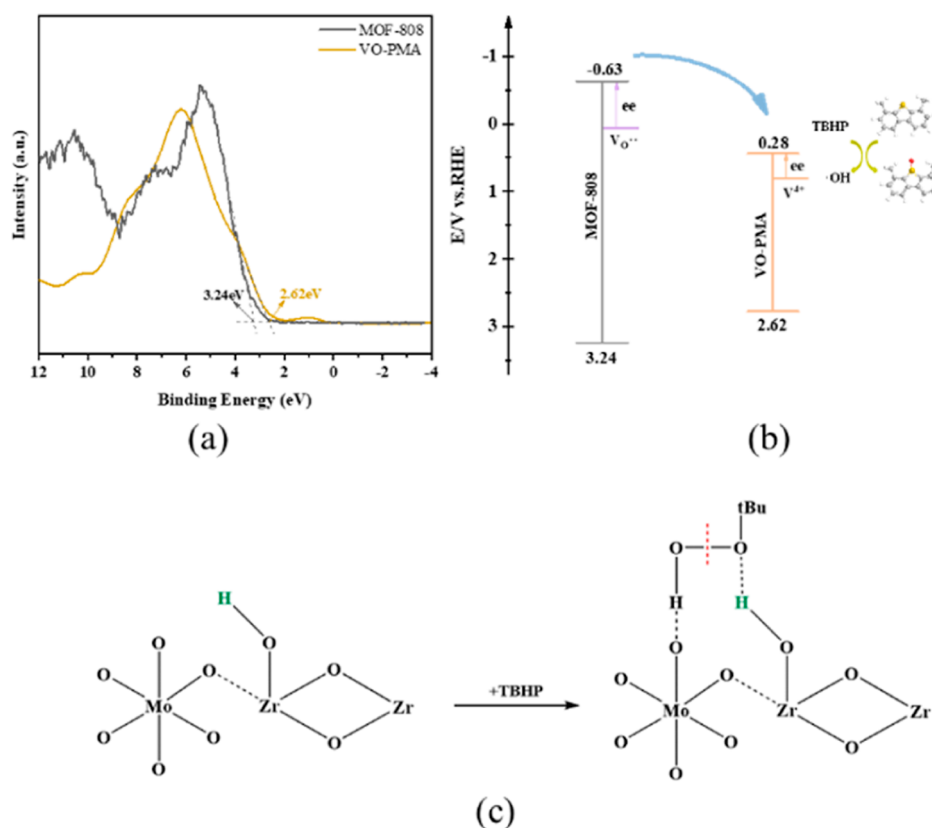


Figure 4. (a) XPS valence band spectra, (b) schematic diagram of the electronic structure, and (c) diagram of the reaction site mechanism.

decreased from 3.16 to 2.16 eV, implying the introduction of V^{4+} and oxygen vacancy defect levels in the forbidden band narrowed the band gap. This result facilitates the subsequent understanding the ODS mechanism with the electronic structure of the composites.

XPS valence band spectra were investigated to study the electron structure of the samples. According to Figure 4a and Table 2, the conduction band (CB) was calculated as -0.63 V (vs RHE) for MOF-808 and 0.28 V (vs RHE) for VO-PMA. The schematic diagram of the electronic structure of VC-VO-PMA/MOF-808 is shown in Figure 4b. MOF-808 has an oxygen vacancy ($V_O^{\bullet\bullet}$) with electron trapping, while VO-PMA has V^{4+} defect levels. The oxygen vacancy energy level is close to the bottom of the MOF-808 conduction band (CB). V^{4+} defect energy level is also near the bottom of VO-PMA. As a result, electrons trapped in oxygen vacancies can be transferred to the CB of MOF-808, resulting in electron aggregating on the CB of MOF-808. The electrons of V^{4+} can also be excited to the CB of VO-PMA as well. In addition, the CB of VO-PMA (0.28 V vs RHE) is lower than that of MOF-808 (-0.63 V vs RHE). Electron transfer occurred from the CB of MOF-808 to the lower CB of VO-PMA, which shows an important synergistic effect between the two for the ODS reaction.

2.2. ODS Activity Evaluation. In order to verify the high ODS activity of the catalyst, DBT and 4,6-DMDBT were dissolved in the simulated oil. In addition, due to the high solubility of the oxidant TBHP in the simulated oil, it is fully in contact with the sulfur containing compounds, further reducing the mass transfer resistance of the reaction. It is

obvious that MOF-808 exhibits little catalytic activity in the reaction in Figure 5a,b. After the loading of PMA or VO-PMA, the activity was significantly improved. It should be noted that the ODS catalytic activity of VO-PMA/MOF-808 is obviously superior to that of PMA/MOF-808. It only takes 40 min to completely remove 4,6-DMDBT. According to the ICP-OES results, the contents of Mo species in VO-PMA/MOF-808 and PMA/MOF-808 are similar; thus, the difference in activity can be explained by the promoting effect of V^{4+} and oxygen vacancy on the ODS reaction. The catalytic activity of the composites obtained after VC modification was further improved. Especially for the VC-VO-PMA/MOF-808 catalyst, it only takes 7 min to remove all DBT, and 12 min to remove all 4,6-DMDBT. The excellent activity of the VC-VO-PMA/MOF-808 catalyst comes from two points. On the one hand, the introduction of V^{4+} can promote the catalytic reaction, and on the other hand, VC modification increases the oxygen defects in the catalyst, providing more active sites for the reaction. To the best of our knowledge, its superior desulfurization performance ranks among the best in the published work. A comparison of related works is given in Table S3.

Considering the porosity of the MOF structure, in order to exclude the effect of adsorption, a desulfurization reaction test was carried out without adding any oxidant, and the results are presented in Figure S8. Under such conditions, almost no DBT and 4,6-DMDBT can be removed even with the addition of VC-VO-PMA/MOF-808 catalyst. Therefore, it can be deduced that the removal of DBT and 4,6-DMDBT is a chemical reaction process rather than adsorption. Furthermore, the catalytic activity of VC-VO-PMA/MOF-808 at 40, 60, and 80 °C was investigated to explore the dynamic characteristics of

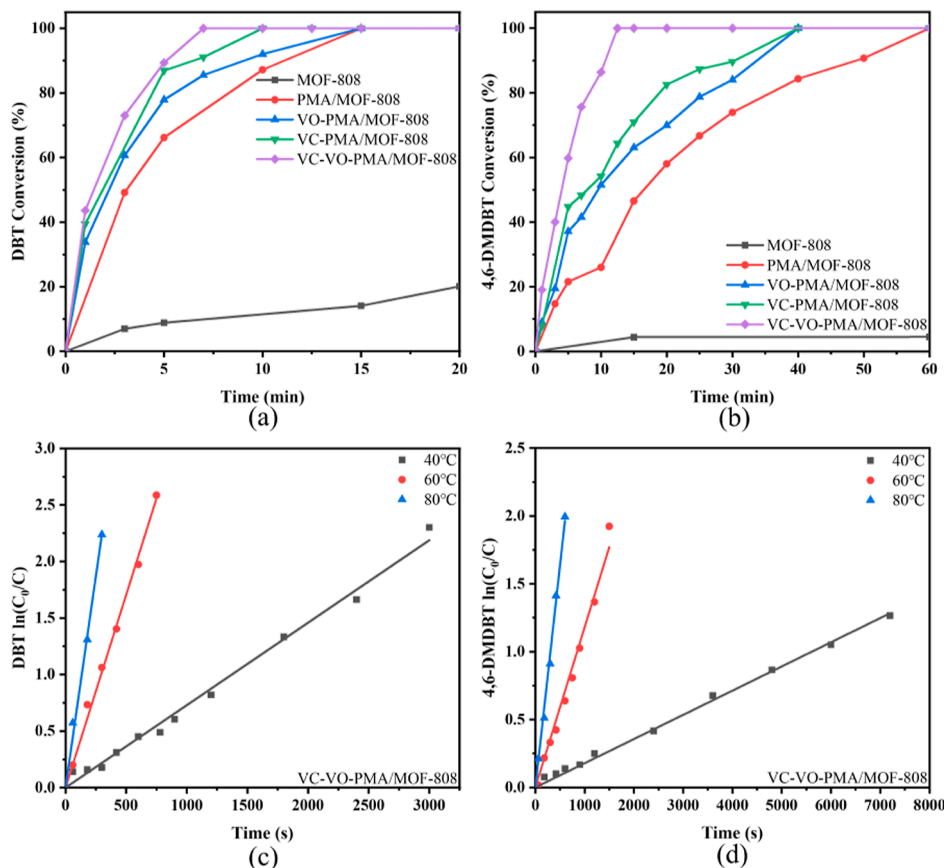


Figure 5. (a) DBT and (b) 4,6-DMDBT conversion over different catalysts at the condition of O/S = 3; Pseudo-first-order reaction for oxidation of (c) DBT and (d) 4,6-DMDBT over VC-VO-PMA/MOF-808.

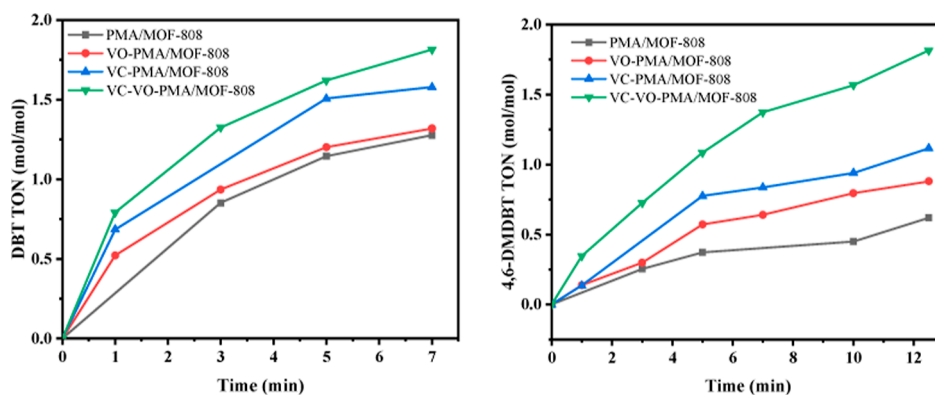


Figure 6. Calculated TON values for the catalysts. Reaction conditions: 500 ppm of DBT and 500 ppm 4,6-DMDBT, 10 g of simulated diesel oil, 20 mg of catalyst, 80 °C, O/S = 3:1.

the reaction. As shown in Figure S9, as the temperature increases, the reaction rate gradually increases, conforming to the general characteristics of chemical reactions. The relationship between the concentration and the reaction time in the reaction process is calculated by eq 2. Plot $\ln(C_0/C)$ against reaction time, in which C_0/C is defined as the ratio of initial sulfur concentration of DBT (4,6-DMDBT)/unreacted sulfur concentration of DBT (4,6-DMDBT). As is given in Figure 5c,d, $\ln(C_0/C)$ –time has a linear relationship. This is the kinetic characteristic of a first-order reaction. This provides evidence that the oxidative removal process of DBT and DMDBT is a pseudo-first-order reaction, and the slope of the line is the k_{ODS} of the reaction at that temperature. In addition,

according to the Arrhenius formula in eq 3, the apparent activation energy (E_a) of the reaction could be calculated by the linear relationship of $\ln k_{\text{ODS}}$ and exact temperature (T) in Figure S10, and the E_a calculations for DBT and 4,6-DMDBT oxidation are 54 and 67 kJ/mol, respectively.

$$\ln \frac{C_0}{C} = k_{\text{ODS}}t \quad (2)$$

$$\ln k_{\text{ODS}} = \ln A - \frac{E_a}{RT} \quad (3)$$

TON value is defined and calculated according to the formula of $\text{TON} = n/m$ (n is the mole of reacted DBT/4,6-

DMDBT per gram of catalyst, m is the mole of Mo atom per gram catalyst). After VC modification, the TON values of PMA/MOF-808 and VC-VO-PMA/MOF-808 increased significantly (Figure 6). The TON value was as high as 1.81 mol/mol for VC-VO-PMA/MOF-808, which was nearly two times that of PMA/MOF-808. It suggests that VC modification leading to the formation of oxygen vacancy and V^{4+} are positive for the ODS activity.

Finally, the regeneration and recycling performance of the catalyst are evaluated in Figure S11. The catalytic performance of VC-VO-PMA/MOF-808 did not decrease in three cycles, and all sulfur compounds in the simulated oil could be removed within 12 min. XRD, IR, XPS results, and TEM images of the used VC-VO-PMA/MOF-808 are given in Figures S12–14. It is obvious that the structure of MOF-808 remains unchanged in the PXRD patterns. The vibration band at 885 cm^{-1} in the IR spectrum proves that PMA Keggin structure still exists. The XPS spectra of the composites did not change. In the TEM image, the catalyst still maintains a completely regular octahedral morphology. The above results point to VC-VO-PMA/MOF-808 as a catalyst with good regeneration ability and cycle stability and also provide a basis for its large-scale application.

2.3. ODS Mechanism. VC-VO-PMA/MOF-808 shows the highest ODS activity, which can be related to its microstructure and electronic structure. First, sufficient amounts of unsaturated Zr sites in the MOF-808 microstructure with a pore diameter of 10 \AA create conditions for anchoring VO-PMA with a molecular size of about 10 \AA to form a Mo–O–Zr bond. Proper porosity provides sufficient channels for reaction substrates and oxidants. Second, the synergistic effect of VO-PMA with exposed Zr sites gives it an advantage in ODS reaction to form V^{4+} and oxygen vacancy as active sites. The main active species in the ODS process is hydroxyl radicals ($\bullet\text{OH}$) produced from the TBHP decomposition as we reported.³⁰ A possible catalytic reaction mechanism was proposed according to the formation of hydroxyl radical active species and Mo–O–Zr active sites. As shown in Figure 4c, the adjacent Mo–O and Zr–OH sites in the formed Mo–O–Zr bond provide the adsorption sites for TBHP oxidant, the oxygen atom in TBHP is linked with the Zr–OH site through hydrogen bonding, and the hydrogen atom in TBHP is linked with the Mo–O bond through hydrogen bonding. In the presence of Mo–O–Zr collaborative catalytic sites, the peroxy –O–O– bond breaks to form hydroxyl radicals. $\bullet\text{OH}$ can easily oxidize the S atom in DBT and 4,6-DMDBT to produce sulfoxides, the high electron density on Mo and V atoms for VC-VO-PMA/MOF-808 is suggested to form $\bullet\text{OH}$ reactive species more easily, thus promoting the ODS reaction.

3. EXPERIMENTAL SECTION

3.1. Synthesis of MOF-808. ZrCl_4 (0.466 g, 2 mmol), trimesic acid (BTC, 0.14 g, 0.66 mmol), N,N -dimethylformamide (DMF, 70 mL), and acetic acid (HAc, 50 mL) were placed in a glass vessel. The mixture was sonicated for 30 min and transferred to a PTFE-lined stainless-steel reactor for 36 h at $120\text{ }^\circ\text{C}$. After the reaction is completed and reduced to room temperature, the mixture is centrifuged, washed thoroughly with DMF, and then dried at $70\text{ }^\circ\text{C}$ for 10 h. The white solid product MOF-808 is obtained.

3.2. Synthesis of VO-PMA. VO-PMA was synthesized according to the synthesis of $[\text{VO}(\text{H}_2\text{O})_5]\text{H}[\text{PMo}_{12}\text{O}_{40}]\cdot 23\text{H}_2\text{O}$ given in the previous research.³⁹ PMA (10 g, 4.85

mmol) was dissolved in 10 mL of water. $\text{Ba}(\text{OH})_2\cdot 8\text{H}_2\text{O}$ (1.56 g, 4.85 mmol) was added slowly to the solution by stirring multiple times. Then, vanadyl sulfate hydrate VOSO_4 (1.25 g, 4.85 mmol) was quickly added to the solution, and the mixture was stirred for 30 min at room temperature. The resulting barium sulfate BaSO_4 precipitate was filtered out, and the solution was kept at $4\text{ }^\circ\text{C}$ in the refrigerator. The dark green solid was obtained by slow recrystallization and was named VO-PMA.

3.3. Synthesis of VO-PMA/MOF-808 and PMA/MOF-808. Disperse 100 mg of MOF-808 and 10 mg of VO-PMA in a mixed solution containing 30 mL of water and 30 mL of ethanol. After 20 min of sonication, the reaction was hydrothermal at $100\text{ }^\circ\text{C}$ for 12 h. When reduced to room temperature, the mixture was centrifuged, washed several times with water and ethanol, and dried in an oven at $70\text{ }^\circ\text{C}$ for 10 h to obtain catalyst VO-PMA/MOF-808. PMA/MOF-808 and VO-PMA/MOF-808 are synthesized in the same way except that VO-PMA is replaced by an equal amount of PMA.

3.4. Synthesis of VC-VO-PMA/MOF-808 and VC-PMA/MOF-808. 100 mg of MOF-808, 10 mg of VO-PMA, and 12 mg of Vitamin C were dispersed in 30 mL of H_2O and 30 mL of ethanol. Subsequent preparation and treatment methods are the same as VO-PMA/MOF-808, and catalyst VC-VO-PMA/MOF-808 was obtained. VC-PMA/MOF-808 are synthesized in the same way with VC-VO-PMA/MOF-808, except that VO-PMA is replaced by an equal amount of PMA.

3.5. Catalytic Reaction. First, dibenzothiophene (DBT) and 4,6-dimethyldibenzothiophene (4,6-DMDBT) were dissolved in n -octane to obtain the simulated oil at concentrations of 500 ppm each. Typically, 10 g of simulated oil and a certain amount of *tert*-butyl hydroperoxide (TBHP) are placed in a round-bottom flask. After slowly heating the flask from room temperature to the target temperature, 20 mg of catalyst is added to the reactor. GC with an FID detector was used to detect the amounts of remaining DBT and 4,6-DMDBT in the solution. Lastly, the samples were centrifuged, washed three times with ethanol, and dried in an oven at $70\text{ }^\circ\text{C}$ for 10 h to obtain the used catalyst.

4. CONCLUSIONS

A series of composite catalysts were obtained by introducing a VO^{2+} group into the phosphomolybdic acid microstructure. Then, it was loaded on MOF-808 and modified with Vitamin C. Surprisingly, the VC-VO-PMA/MOF-808 completely removed DBT and 4,6-DMDBT from the simulated oil in 12 min. The oxygen vacancy and V^{4+} generated by VC modification in VC-VO-PMA/MOF-808 have a positive effect on the ODS reaction. This study provides a new perspective for the development of readily available and efficient ODS catalysts.

■ ASSOCIATED CONTENT

Supporting Information

The Supporting Information is available free of charge at <https://pubs.acs.org/doi/10.1021/acsomega.3c05458>.

Characterization; TEM images; SEM images; XRD pattern; nitrogen adsorption–desorption isotherms and pore size distribution curves; TGA curves; XPS spectra; acid–base titration; DBT and 4,6-DMDBT conversion; Arrhenius plots; stability; IR spectra; BET surface and pore volume; and activity comparison chart (PDF)

AUTHOR INFORMATION

Corresponding Author

Dan-Hong Wang – TKL of Metal and Molecule Based Material Chemistry, School of Materials Science and Engineering, Nankai University, Tianjin 300350, China; orcid.org/0000-0001-6780-3033; Phone: +86-13821127707; Email: dhwang@nankai.edu

Authors

Yi Ping – TKL of Metal and Molecule Based Material Chemistry, School of Materials Science and Engineering, Nankai University, Tianjin 300350, China
Meng-Ya Zong – TKL of Metal and Molecule Based Material Chemistry, School of Materials Science and Engineering, Nankai University, Tianjin 300350, China
Zhe Zhao – TKL of Metal and Molecule Based Material Chemistry, School of Materials Science and Engineering, Nankai University, Tianjin 300350, China
Chuan-Jiao Wang – TKL of Metal and Molecule Based Material Chemistry, School of Materials Science and Engineering, Nankai University, Tianjin 300350, China

Complete contact information is available at:
<https://pubs.acs.org/10.1021/acsomega.3c05458>

Author Contributions

Yi Ping: investigation, formal analysis, visualization, writing—original draft, and validation; Meng-Ya Zong: investigation, formal analysis, visualization, and writing—original draft; Zhe Zhao: investigation and validation; Chuan-Jiao Wang: validation; and Dan-Hong Wang: writing—review and editing, project administration, and funding acquisition.

Notes

The authors declare no competing financial interest.

ACKNOWLEDGMENTS

This work was supported by the 111 project (B18030) from China. The authors also acknowledge the financial support of the Haihe Laboratory of Sustainable Chemical Transformations (YYJC202101).

REFERENCES

- (1) Haruna, A.; Merican Aljunid Merican, Z.; Gani Musa, S.; Abubakar, S. Sulfur Removal Technologies from Fuel Oil for Safe and Sustainable Environment. *Fuel* **2022**, *329*, 125370.
- (2) Ullah, L.; Zhao, G.; Ma, J.-X.; Usman, M.; Khan, R.; Hedin, N. Pd-Promoted Heteropolyacid on Mesoporous Zirconia as a Stable and Bifunctional Catalyst for Oxidation of Thiophenes. *Fuel* **2022**, *310*, 122462.
- (3) Chen, L.; Ren, J.-T.; Yuan, Z.-Y. Increasing the Utilization of SiBeta Support to Anchor Dual Active Sites of Transition Metal and Heteropolyacids for Efficient Oxidative Desulfurization of Fuel. *Appl. Catal., B* **2022**, *305*, 121044.
- (4) Jiang, W.; An, X.; Xiao, J.; Yang, Z.; Liu, J.; Chen, H.; Li, H.; Zhu, W.; Li, H.; Dai, S. Enhanced Oxygen Activation Achieved by Robust Single Chromium Atom-Derived Catalysts in Aerobic Oxidative Desulfurization. *ACS Catal.* **2022**, *12* (14), 8623–8631.
- (5) Xiong, J.; Li, J.; Chen, C.; Jiang, W.; Zhu, W.; Li, H.; Di, J. Universal Strategy Engineering Grain Boundaries for Catalytic Oxidative Desulfurization. *Appl. Catal., B* **2022**, *317*, 121714.
- (6) Hao, L.; Hurlock, M. J.; Ding, G.; Zhang, Q. Metal-Organic Frameworks Towards Desulfurization of Fuels. *Top. Curr. Chem.* **2020**, *378* (1), 17.
- (7) Li, S.-W.; Gao, R.-M.; Zhao, J. Deep Oxidative Desulfurization of Fuel Catalyzed by Modified Heteropolyacid: The Comparison Performance of Three Kinds of Ionic Liquids. *ACS Sustainable Chem. Eng.* **2018**, *6* (11), 15858–15866.
- (8) Yue, S.; Song, W.; Pan, S.; Liu, D.; Li, C.; Zang, J.; Nan, J.; Gui, J. Efficient Oxidative Desulfurization over $[\text{Mo}_8\text{O}_{26}]^{4-}$ -Based Hybrids: Phase Transfer Catalysis. *Energy Fuels* **2023**, *37* (13), 8988–8998.
- (9) Rezvani, M. A.; Khandan, S.; Sabahi, N. Oxidative Desulfurization of Gas Oil Catalyzed by $(\text{TBA})_4\text{PW}_{11}\text{Fe@PbO}$ as an Efficient and Recoverable Heterogeneous Phase-Transfer Nanocatalyst. *Energy Fuels* **2017**, *31* (5), 5472–5481.
- (10) Boshagh, F.; Rahmani, M.; Zhu, W. Recent Advances and Challenges in Developing Technological Methods Assisting Oxidative Desulfurization of Liquid Fuels: A Review. *Energy Fuels* **2022**, *36* (21), 12961–12985.
- (11) Boshagh, F.; Rahmani, M.; Rostami, K.; Yousefifar, M. Key Factors Affecting the Development of Oxidative Desulfurization of Liquid Fuels: A Critical Review. *Energy Fuels* **2022**, *36* (1), 98–132.
- (12) Ye, G.; Wang, H.; Zeng, X.; Wang, L.; Wang, J. Defect-Rich Bimetallic UiO-66(Hf-Zr): Solvent-Free Rapid Synthesis and Robust Ambient-Temperature Oxidative Desulfurization Performance. *Appl. Catal., B* **2021**, *299*, 120659.
- (13) Wu, C.; Sun, Z.; Ye, C.; Qi, Z.; Chen, J.; Huang, Z.; Qiu, T. Encapsulation of HPW and Preparation of Composites Rich in Zr-Defects by Manual Grinding: Synergistic Catalysis for Efficient Oxidative Desulfurization at Room Temperature. *Chem. Eng. J.* **2023**, *451*, 138906.
- (14) Chen, L.; Ren, J.-T.; Yuan, Z.-Y. Identifying the Dominant Effect of Electron-Feeding on Molybdenum Phosphonates to Decipher the Activity Origin for Oxidative Desulfurization of Fuel. *Chem. Eng. J.* **2022**, *450*, 138330.
- (15) Haruna, A.; Merican, Z. M. A.; Musa, S. G.; Rahman, M. B. A. MOF-808(Zr)-Supported with Keggin Polyoxometalates as an Efficient Oxidative Desulfurization Catalyst. *J. Taiwan Inst. Chem. Eng.* **2023**, *147*, 104919.
- (16) Musa, S. G.; Aljunid Merican, Z. M.; Haruna, A. Investigation of Isotherms and Isotheric Heat of Adsorption for PW11@HKUST-1 Composite. *J. Solid State Chem.* **2022**, *314*, 123363.
- (17) Peng, Y.-L.; Liu, J.; Zhang, H.-F.; Luo, D.; Li, D. A Size-Matched POM@MOF Composite Catalyst for Highly Efficient and Recyclable Ultra-Deep Oxidative Fuel Desulfurization. *Inorg. Chem. Front.* **2018**, *5* (7), 1563–1569.
- (18) Ghubayra, R.; Yahya, R.; Kozhevnikova, E. F.; Kozhevnikov, I. V. Oxidative Desulfurization of Model Diesel Fuel Catalyzed by Carbon-Supported Heteropoly Acids: Effect of Carbon Support. *Fuel* **2021**, *301*, 121083.
- (19) Zhang, B.; Sun, G.; Ding, S.; Asakura, H.; Zhang, J.; Sautet, P.; Yan, N. Atomically Dispersed Pt1-Polyoxometalate Catalysts: How Does Metal-Support Interaction Affect Stability and Hydrogenation Activity? *J. Am. Chem. Soc.* **2019**, *141* (20), 8185–8197.
- (20) Samaniyan, M.; Mirzaei, M.; Khajavian, R.; Eshtiagh-Hosseini, H.; Streb, C. Heterogeneous Catalysis by Polyoxometalates in Metal-Organic Frameworks. *ACS Catal.* **2019**, *9* (11), 10174–10191.
- (21) Hülsey, M. J.; Zhang, B.; Ma, Z.; Asakura, H.; Do, D. A.; Chen, W.; Tanaka, T.; Zhang, P.; Wu, Z.; Yan, N. In Situ Spectroscopy-Guided Engineering of Rhodium Single-Atom Catalysts for CO Oxidation. *Nat. Commun.* **2019**, *10* (1), 1330.
- (22) Zhou, S.; He, J.; Wu, P.; He, L.; Tao, D.; Lu, L.; Yu, Z.; Zhu, L.; Chao, Y.; Zhu, W. Metal-Organic Framework Encapsulated High-Loaded Phosphomolybdic Acid: A Highly Stable Catalyst for Oxidative Desulfurization of 4,6-Dimethylidibenzothiophene. *Fuel* **2022**, *309*, 122143.
- (23) Abazari, R.; Esrafil, L.; Morsali, A.; Wu, Y.; Gao, J. PMo12@UiO-67 Nanocomposite as a Novel Non-Leaching Catalyst with Enhanced Performance Durability for Sulfur Removal from Liquid Fuels with Exceptionally Diluted Oxidant. *Appl. Catal., B* **2021**, *283*, 119582.
- (24) Chang, X.; Yang, X.-F.; Qiao, Y.; Wang, S.; Zhang, M.-H.; Xu, J.; Wang, D.-H.; Bu, X.-H. Confined Heteropoly Blues in Defected Zr-

MOF (Bottle Around Ship) for High-Efficiency Oxidative Desulfurization. *Small* **2020**, *16* (14), 1906432.

(25) Chu, L.; Guo, J.; Huang, Z.; Yang, H.; Yang, M.; Wang, G. Excellent Catalytic Performance over Acid-Treated MOF-808(Ce) for Oxidative Desulfurization of Dibenzothiophene. *Fuel* **2023**, *332*, 126012.

(26) Mao, S.-X.; Zhou, Q.-H.; Guo, H.-L.; Du, M.; Zhu, W.-S.; Li, H.-M.; Pang, J.-Y.; Dang, D.-B.; Bai, Y. Porous Phosphomolybdate-Based Poly(Ionic Liquid) Hybrids with Reversible Water Absorption for Enhancement of Oxidative Desulfurization. *Fuel* **2023**, *333*, 126392.

(27) Leng, Y.; Ge, H.; Zhou, C.; Wang, J. Direct Hydroxylation of Benzene with Hydrogen Peroxide over Pyridine-Heteropoly Compounds. *Chem. Eng. J.* **2008**, *145* (2), 335–339.

(28) Zhang, M.; Liu, J.; Li, H.; Wei, Y.; Fu, Y.; Liao, W.; Zhu, L.; Chen, G.; Zhu, W.; Li, H. Tuning the Electrophilicity of Vanadium-Substituted Polyoxometalate Based Ionic Liquids for High-Efficiency Aerobic Oxidative Desulfurization. *Appl. Catal., B* **2020**, *271*, 118936.

(29) Rajendran, A.; Cui, T.; Fan, H.; Yang, Z.; Feng, J.; Li, W. A Comprehensive Review on Oxidative Desulfurization Catalysts Targeting Clean Energy and Environment. *J. Mater. Chem. A* **2020**, *8* (5), 2246–2285.

(30) Deng, C.; Wu, P.; Li, H.; Zhu, H.; Chao, Y.; Tao, D.; Chen, Z.; Hua, M.; Liu, J.; Liu, J.; Zhu, W. Engineering Polyhedral High Entropy Oxide with High-Index Facets via Mechanochemistry-Assisted Strategy for Efficient Oxidative Desulfurization. *J. Colloid Interface Sci.* **2023**, *629*, 569–580.

(31) Zou, J.; Lin, Y.; Wu, S.; Zhong, Y.; Yang, C. Molybdenum Dioxide Nanoparticles Anchored on Nitrogen-Doped Carbon Nanotubes as Oxidative Desulfurization Catalysts: Role of Electron Transfer in Activity and Reusability. *Adv. Funct. Mater.* **2021**, *31* (22), 2100442.

(32) Wang, S.; Zhang, X.; Chang, X.; Zong, M.-Y.; Fan, C.-Z.; Guo, D.-X.; Xu, J.; Wang, D.-H.; Bu, X.-H. Rational Design of Ionic V-MOF with Confined Mo Species for Highly Efficient Oxidative Desulfurization. *Appl. Catal., B* **2021**, *298*, 120594.

(33) Lin, Z.-J.; Zheng, H.-Q.; Chen, J.; Zhuang, W.-E.; Lin, Y.-X.; Su, J.-W.; Huang, Y.-B.; Cao, R. Encapsulation of Phosphotungstic Acid into Metal-Organic Frameworks with Tunable Window Sizes: Screening of PTA@MOF Catalysts for Efficient Oxidative Desulfurization. *Inorg. Chem.* **2018**, *57* (20), 13009–13019.

(34) Haruna, A.; Merican, Z. M. A.; Musa, S. G. Facile Fabrication of PTA@MOF-808H Nanocomposites in Acidic Media Employing Hydrogen Peroxide for Catalytic Oxidative Desulfurization of Fuel Oil. In *Proceedings of the 1st International Conference of New Energy*; Othman, M. B., Abdul Karim, S. A.; Wilfred, C. D.; Lee, K. C.; Sokkalingam, R., Eds.; Springer Proceedings in Energy; Springer Nature: Singapore, 2023; pp 115–123.

(35) Tu, Y.; Li, T.; Yu, G.; Wei, L.; Ta, L.; Zhou, Z.; Ren, Z. Study on Modification and Desulfurization Performance of a Molybdenum-Based Catalyst. *Energy Fuels* **2019**, *33* (9), 8503–8510.

(36) Haruna, A.; Merican, Z. M. A.; Musa, S. G. Remarkable Stability and Catalytic Performance of PW11M@MOF-808 (M = Mn and Cu) Nanocomposites for Oxidative Desulfurization of Fuel Oil. *Mol. Catal.* **2023**, *541*, 113079.

(37) Zhang, X.; Zhang, Z.; Zhang, B.; Yang, X.; Chang, X.; Zhou, Z.; Wang, D.-H.; Zhang, M.-H.; Bu, X.-H. Synergistic Effect of Zr-MOF on Phosphomolybdic Acid Promotes Efficient Oxidative Desulfurization. *Appl. Catal., B* **2019**, *256*, 117804.

(38) Mu, J.; Liu, J.; Ran, Z.; Arif, M.; Gao, M.; Wang, C.; Ji, S. Critical Role of CUS in the Au/MOF-808(Zr) Catalyst for Reaction of CO₂ with Amine/H₂ via N-Methylation and N-Formylation. *Ind. Eng. Chem. Res.* **2020**, *59* (14), 6543–6555.

(39) Bayer, R.; Marchal, C.; Liu, F. X.; Tézé, A.; Hervé, G. ESR Characterization of V⁴⁺ as a Counter-Ion of the 12-Molybdophosphate. Influence of Thermal Treatments. *J. Mol. Catal. A: Chem.* **1996**, *110* (2), 65–76.

(40) Ogunlaja, A. S.; Khene, S.; Antunes, E.; Nyokong, T.; Torto, N.; Tshentu, Z. R. The Development of Catalytic Oxovanadium(IV)-

Containing Microspheres for the Oxidation of Various Organosulfur Compounds. *Appl. Catal., A* **2013**, *462–463*, 157–167.

(41) Parsaei, M.; Akhbari, K. Synthesis and Application of MOF-808 Decorated with Folic Acid-Conjugated Chitosan as a Strong Nanocarrier for the Targeted Drug Delivery of Quercetin. *Inorg. Chem.* **2022**, *61* (48), 19354–19368.

(42) Zhang, W.; Bu, A.; Ji, Q.; Min, L.; Zhao, S.; Wang, Y.; Chen, J. PKa-Directed Incorporation of Phosphonates into MOF-808 via Ligand Exchange: Stability and Adsorption Properties for Uranium. *ACS Appl. Mater. Interfaces* **2019**, *11* (37), 33931–33940.

(43) Furukawa, H.; Gándara, F.; Zhang, Y.-B.; Jiang, J.; Queen, W. L.; Hudson, M. R.; Yaghi, O. M. Water Adsorption in Porous Metal-Organic Frameworks and Related Materials. *J. Am. Chem. Soc.* **2014**, *136* (11), 4369–4381.

(44) Klet, R. C.; Liu, Y.; Wang, T. C.; Hupp, J. T.; Farha, O. K. Evaluation of Brønsted Acidity and Proton Topology in Zr- and Hf-Based Metal-Organic Frameworks Using Potentiometric Acid-Base Titration. *J. Mater. Chem. A* **2016**, *4* (4), 1479–1485.

(45) DeStefano, M. R.; Islamoglu, T.; Garibay, S. J.; Hupp, J. T.; Farha, O. K. Room-Temperature Synthesis of UiO-66 and Thermal Modulation of Densities of Defect Sites. *Chem. Mater.* **2017**, *29* (3), 1357–1361.